Soft Matter

PAPER

View Article Online
View Journal | View Issue

Cite this: *Soft Matter*, 2016, 12, 5937

Dimeric peptides with three different linkers self-assemble with phospholipids to form peptide nanodiscs that stabilize membrane proteins

Andreas N. Larsen,[a] Kasper K. Sørensen,[b] Nicolai T. Johansen,[a] Anne Martel,[c] Jacob J. K. Kirkensgaard,[a] Knud J. Jensen,[b] Lise Arleth*[a] and Søren Roi Midtgaard*[a]

Three dimers of the amphipathic α-helical peptide 18A have been synthesized with different interhelical linkers inserted between the two copies of 18A. The dimeric peptides were denoted 'beltides' where Beltide-1 refers to the 18A-dimer without a linker, Beltide-2 is the 18A-dimer with proline (Pro) as a linker and Beltide-3 is the 18A-dimer linked by two glycines (Gly–Gly). The self-assembly of the beltides with the phospholipid DMPC was studied with and without the incorporated membrane protein bacteriorhodopsin (bR) through a combination of coarse-grained MD simulations, size-exclusion chromatography (SEC), circular dichroism (CD) spectroscopy, small-angle scattering (SAS), static light scattering (SLS) and UV-Vis spectroscopy. For all three beltides, MD and combined small-angle X-ray and -neutron scattering were consistent with a disc structure composed by a phospholipid bilayer surrounded by a belt of peptides and with a total disc diameter of approximately 10 nm. CD confirmed that all three beltides were α-helical in the free form and with DMPC. However, as shown by SEC the different interhelical linkers clearly led to different properties of the beltides. Beltide-3, with the Gly–Gly linker, was very adaptable such that peptide nanodiscs could be formed for a broad range of different peptide to lipid stoichiometries and therefore also possible disc-sizes. On the other hand, both Beltide-2 with the Pro linker and Beltide-1 without a linker were less adaptable and would only form discs of certain peptide to lipid stoichiometries. SLS revealed that the structural stability of the formed peptide nanodiscs was also highly affected by the linkers and it was found that Beltide-1 gave more stable discs than the other two beltides. With respect to membrane protein stabilization, each of the three beltides in combination with DMPC stabilizes the seven-helix transmembrane protein bacteriorhodopsin significantly better than the detergent octyl glucoside, but no significant difference was observed between the three beltides. We conclude that adaptability, size, and structural stability can be tuned by changing the interhelical linker while maintaining the properties of the discs with respect to membrane protein stabilization.

Received 25th February 2016,
Accepted 1st June 2016

DOI: 10.1039/c6sm00495d

www.rsc.org/softmatter

Introduction

Membrane proteins have attracted great pharmaceutical interest since they are the specific targets of more than 50% of all drugs.[1] However, only 1–2% of the known protein structures in the Protein Data Bank are from membrane proteins. One reason is that membrane proteins rely strongly on a native-like amphiphilic environment to be stable, functional and accessible by crystallization for high-resolution diffraction experiments. This has motivated many studies on different reconstitution systems, from detergent micelles and amphipols[2] to membrane mimicking systems such as liposomes, bicelles,[3] SMALPs[4] and nanodiscs.[5] In the present study we investigate a new type of nanodisc system based on dimers of the peptide 18A with different interhelical linkers.

The conventional nanodisc system is composed of a lipid bilayer, with the hydrophobic side screened by a double belt consisting of two amphiphilic membrane scaffolding proteins (MSPs) derived from human apoA1.[5,6] MSP nanodiscs stabilize membrane proteins well and are highly homogeneous from a structural point of view.[7] This is essential for structural studies such as small-angle scattering and single particle electron microscopy. However, reconstitution of membrane proteins in MSP nanodiscs is challenging from a sample handling point of view, and the system has limited flexibility with respect to the size of the membrane proteins that can be incorporated due to the fixed size of the MSP belt. We have therefore previously investigated

[a] Niels Bohr Institute, University of Copenhagen, Denmark. E-mail: arleth@nbi.ku.dk, soromi@nbi.ku.dk
[b] Department of Chemistry, University of Copenhagen, Denmark
[c] Institut Laue-Langevin, Grenoble, France

nanodiscs with repeated, unlinked peptide units as a possible alternative to MSP, and showed that the amphipathic peptide, 18A, self-assembles with DMPC to form well-defined peptide nanodiscs with a diameter of about 100 Å, which can stabilize the seven-helix transmembrane protein bacteriorhodopsin well.[8] The 18A peptide was first introduced by Segrest *et al.*[9] and variants have been studied extensively[10–13] due to their potential as a therapy to prevent atherosclerosis.[14] Also NMR studies of 18A with DMPC were previously performed to elucidate the structure of the discs.[10,15]

In our previous study,[8] the formed 18A discs were found to be unstable over time and reorganize into larger particles. In this study we hypothesize that the structural stability as well as other properties, such as overall structure, homogeneity and ability to stabilize membrane proteins can be tuned by using dimers of 18A with different interhelical linkers, such that the formed peptide nanodiscs can be optimized for specific purposes. Therefore, we have investigated how dimers of 18A with three different types of linkers self-assembled with DMPC to form peptide nanodiscs. The belt peptides, which we denoted "beltides", were Beltide-1, which contained two copies of 18A connected directly *via* a standard peptide-bond, *i.e.* with no additional linker, Beltide-2 with the 18A-dimer linked by proline (Pro), and Beltide-3 with the 18A-dimer linked by a double glycine (Gly–Gly) linker residue (see Fig. 1). The choice of the Pro and Gly–Gly motifs were motivated by their presence as linkers in the amino acid sequence of human apoA1, and because of their helix-breaking properties.[16] They were expected to provide 18A-dimers with different degrees of flexibility. The helical structure of Beltide-1 is not explicitly interrupted so this peptide was expected to be rigid. Pro is the most abundant linker in apoA1 and is found in seven out of ten helical segments. It induces a ~30° kink and is helix-unwinding,[17] such that the α-helix does not twist 100° as usual, but only ~30°. Ramachandran plots[18] show how Pro limits the core regions for the dihedral angles before and after the residue, meaning that Beltide-2 has a limited flexibility. A double Gly motif is found between the seventh and the eighth helix in apoA1. Gly has no side-chain, and, excluding Pro, it has the lowest propensity for helix formation,[16] so the Gly–Gly motif is expected to locally break the helical structure such that adjacent helical segments can move almost freely with respect to each other,[18] hence Beltide-3 was expected to be very flexible. Peptides similar to Beltides-1 and -2, but without the amidation and acetylation of the ends, have been previously studied by circular dichroism and revealed a helical content of respectively 89 and 73% when associated with DMPC,[19] consistent with the helix-breaking properties of Pro in Beltide-2. Beltide-2 in complex with DMPC has furthermore been studied by negative stain electron microscopy (EM) and found to form discoidal particles with a diameter of ~90 Å[10] at a 1 : 1 weight ratio. Several analogous peptide:phospholid systems have been investigated by EM, and they all form discoidal particles.[13,20–22] A recent study investigated an asymmetric version of Beltide-2 in complex with POPC and showed that these particles were more temperature resistant than 4F:POPC particles,[23] with 4F being 18A with the two leucines (L) replaced by phenylalanines (F). To our knowledge, no studies have been performed on Beltide-3.

Our experimental study of the self-assembly and final structure of the peptide nanodiscs was based on size exclusion chromatography (SEC), circular dichroism (CD) spectroscopy, and combined small-angle X-ray- and neutron scattering (SAXS and SANS). The SAXS and SANS combination is particularly useful for these types of particles due to their internal multiple scattering contrasts. Coarse-grained molecular dynamics (MD) simulations were used to obtain further insight into the self-assembly process of the peptide nanodiscs. The time dependent structural stability of the formed peptide nanodiscs was studied by time-resolved static light scattering. Throughout the study, results on 18A nanodiscs from our previous work[8] were used as reference and the present experiments were performed under the same conditions, allowing for a direct comparison. As a part of the study, bacteriorhodopsin was reconstituted into the beltide nanodiscs to investigate their ability to stabilize a transmembrane protein. It was found that the different flexibilities provided by the linkers were directly reflected in their self-assembly and in the structure of the formed beltide nanodiscs, as well as in the structural stability of the discs. It was also found that all Beltides-1, 2 and 3 stabilize bacteriorhodopsin very well and significantly better than the detergent octyl glucoside (OG). No internal difference between the three beltides was observed with respect to membrane protein stabilization.

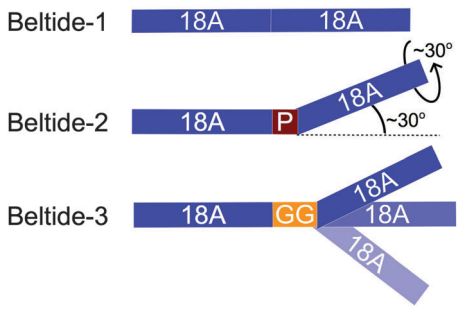

Fig. 1 Sketch of the three dimer belt peptides (beltides) with, respectively, no linker, Pro as a linker and a double Gly motif as a linker. The linkers were expected to alter the structural flexibility of the beltides. Beltide-1 was expected to be rigid, Beltide-2 to have a limited flexibility with an induced kink of ~30° and a fixed helix-unwinding twist, and Beltide-3 was expected to be very flexible.

Materials and methods

Peptide synthesis

The amino acid sequence of the 18A amphipathic helical peptide is DWLKAFYDKVAEKLKEAF. For this study the beltides were acetylated at the N-terminus and amidated at the C-terminus.[21] The two-helix peptides were Beltide-1 with two copies of 18A with no linker, Beltide-2 with two copies of 18A linked by Pro, and Beltide-3 with two copies of 18A linked by Gly–Gly, see Fig. 1. The peptides were synthesized by solid-phase peptide synthesis (SPPS) on an automated peptide synthesizer (Syro II, Biotage) on a TentaGel S Rink Amide 0.24 mmol g^{-1} (Rapp Polymere GmbH)

resin with 9-fluorenylmethyloxycarbonyl (Fmoc) for protection of N^{α}-amino groups and purified using RP-HPLC (Dionex Ultimate 3000 system) with a preparative C18 column (FeF Chemicals, 200 Å 10 μm C18 particles, 2.1 × 200 mm). The purity of the peptides was evaluated by analytical high-performance liquid chromatography (HPLC), and the identification was carried out by electrospray ionization mass spectrometry (ESI-MS) (MSQ Plus Mass Spectrometer, Thermo). The synthesis was the same as in our previous work[8] with the exception of the modified amino acid sequences.

- Beltide-1 ('18A'–'18A')
  Ac-DWLKAFYDKVAEKLKEAF-DWLKAFYDKVAEKLKEAF-NH_2;
  Yield after purification 10–15%; chemical formula: $C_{212}H_{315}N_{47}O_{55}$; molar weight: 4425.34 Da;
  ESI-MS, found masses: *m*/*z*: 1475.7 $[M + 3H]^{3+}$, 1106.4 $[M + 4H]^{4+}$, 885.5 $[M + 5H]^{5+}$, 737.6 $[M + 6H]^{6+}$, 632.8 $[M + 7H]^{7+}$
- Beltide-2 ('18A'-Pro-'18A')
  Ac-DWLKAFYDKVAEKLKEAF-P-DWLKAFYDKVAEKLKEAF-NH_2;
  Yield after purification 10–15%; chemical formula: $C_{217}H_{322}N_{48}O_{56}$; molar weight: 4520.38 Da;
  ESI-MS, found masses: *m*/*z*: 1508.5 $[M + 3H]^{3+}$, 1331.8 $[M + 4H]^{4+}$, 905.5 $[M + 5H]^{5+}$, 754.8 $[M + 6H]^{6+}$
- Beltide-3 ('18A'-Gly–Gly-'18A')
  Ac-DWLKAFYDKVAEKLKEAF-GG-DWLKAFYDKVAEKLKEAF-NH_2;
  Yield after purification 5–10%; chemical formula: $C_{216}H_{321}N_{49}O_{57}$; molar weight: 4539.37 Da;
  ESI-MS, found masses: *m*/*z*: 1513.0 $[M + 3H]^{3+}$, 1135.1 $[M + 4H]^{4+}$, 908.4 $[M + 5H]^{5+}$, 757.0 $[M + 6H]^{6+}$, 649.2 $[M + 7H]^{7+}$.

Bacteriorhodopsin purification

Bacteriorhodopsin (bR) was produced and purified as described in previously published work.[8,24,25] Briefly, salt media were inoculated with *H. salinarium*. After growth, the cells were pelleted and washed in salt buffer. The cells were resuspended in Milli-Q H_2O (MQ). DNase (Sigma) was added, and the solution was left for stirring over night. Cell debris was spun down, the supernatant was transferred to centrifuge tubes, and the membranes were pelleted. The supernatant was discarded, and the pellet was resuspended in MQ and spun down further two times to remove impurities. Isolated membranes were resuspended in a minimum amount of MQ and carefully layered on top of a sucrose gradient. After centrifugation, the band containing the purple membrane was extracted and dialyzed against 25 mM phosphate buffer pH 7.4 to remove sucrose. Octyl glucoside (OG, Applichem) was added to the purple membrane sample to obtain a weight ratio of detergent to bR of ~20, and the sample diluted to obtain a final OG concentration of 40 mM. The solution was lightly sonicated. The bR was loaded onto a Superdex 200 10 : 300 column (GE healthcare) equilibrated in 25 mM phosphate buffer pH 7.4 and 40 mM OG. Fractions containing monomeric bR were collected, concentrated, flash frozen and stored at −80 °C.

Self-assembly of peptide nanodiscs

The peptide dissolved in methanol was mixed with 1,2-dimyristoyl-*sn-glycero*-3-phosphatidylcholine (DMPC). Samples were prepared in stoichiometries ranging from 3 to 43 phospholipids per peptide. This corresponds to weight ratios from (1 : 0.5) to (1 : 6.5). Samples with no phospholipids were also prepared in order to study the self-assembly of the peptides alone. The samples were dried under a stream of nitrogen to a thin film on the inside of sample vials, and subsequently lyophilized overnight to ensure that all residual methanol and chloroform had evaporated. The samples were then rehydrated in an aqueous buffer of 5 mM KH_2PO_4 to a final peptide concentration of 3.3 mM and incubated at 37 °C overnight. The temperature was chosen in accordance with previous work[8] and is well above the phase transition temperature of DMPC at 24 °C. However, 18A nanodiscs with DMPC could also self-assemble at RT (data not shown). The samples were applied on an ÄKTA purifier with a Superdex 200 column equilibrated in 1× Phosphate Buffered Saline (PBS) and absorption at 280 nm was monitored. SEC was performed at room temperature.

Bacteriorhodposin (bR) was reconstituted in the peptide nanodiscs by adding bR in 25 mM phosphate buffer pH 7.4 and 40 mM OG to the dry peptide–lipid film instead of KH_2PO_4. The peptide–lipid stoichiometries were 1 : 19.6, 1 : 10.0, and 1 : 16.7 for Beltides-1, -2, and -3 respectively. This was incubated at room temperature for 15 min before applying to the Superdex 200 column equilibrated in 1× PBS. Absorption at 280 and 550 nm was monitored.

Circular dichroism

Beltides and freshly prepared beltide nanodiscs with the optimal DMPC:beltide stoichiometry were diluted in PBS to a final concentration of ~10 μM while kept cold. 18A and 18A nanodiscs were diluted to ~20 μM. Far UV CD spectra were acquired on a Jasco J815 CD spectrometer equipped with a variable temperature sample holder controlled by a Peltier element. Data were collected in a 1 mm Hellma quartz cuvette at 10 °C with a scan rate of 20 nm min^{-1}, 2 s digital integration time and 1 nm data pitch. Eight spectra were recorded and subsequently averaged and buffer subtracted. CD (mdeg) was converted to mean residual ellipticity with the relation

$$[\theta]_{\mathrm{MRE}} = \frac{\theta \cdot M_{\mathrm{MRE}}}{10 \cdot c \cdot l} \quad (1)$$

where θ is the measured ellipticity in mdeg, M_{MRE} is the molecular weight divided by the number of peptide bonds, c is the mass concentration, and l is the path length in cm. The concentration was determined from the absorbance at 280 nm measured on a VWR UV-1600PC spectrophotometer in a 1 cm Hellma quartz cuvette.

The percentage of helix was estimated from the mean residual ellipticity at 222 nm as described elsewhere.[26–28] The standard error of the mean was computed from the eight spectra obtained for each sample, respectively.

Small-angle X-ray- and neutron scattering (SAXS and SANS)

Samples were measured using SAXS and SANS at, respectively, the BM29 BioSAXS beamline[29] at the European Synchrotron Radiation Facility (ESRF) and at the D11 beamline[30] at the

Institute Laue-Langevin (ILL). Both facilities are located in Grenoble, France. SAXS samples were measured in 100% H_2O based buffers at 10 °C, using an X-ray wavelength λ of 0.99 Å and the standard settings of the instrument,[31] which provide a q-range from 0.0046 to 0.45 Å^{-1}. The data were absolute calibrated with water as standard. Samples for SANS were applied to 2 mm Hellma Quartz cuvettes and measured in 100% D_2O based buffers at 10 °C, using a neutron wavelength λ of 6.0 Å ± 10% (FWHM). SANS data intensity was calibrated to absolute values using the flux of the direct beam. The SANS measurements were performed at two sample-detector distances to cover the relevant q-range: 9.5 m (0.007–0.071 Å^{-1}) and 1.5 m (0.05–0.42 Å^{-1}). In both experiments, the 2D data were azimuthally averaged, normalized and background subtracted to yield the scattering intensity $I(q)$, where the scattering vector q is defined as $q = (4\pi/\lambda)\sin\theta$ and 2θ is the scattering angle. Pair distance distribution functions $p(r)$ were obtained by indirect Fourier transformation performed using BayesApp[32] (www.bayesapp.org).

Samples were stored on ice after preparation and were centrifuged at 14 000 rpm for 15 min to avoid large aggregates. Peptide concentrations were determined from their absorption at 280 nm measured on a NanoDrop 1000 spectrophotometer (Thermo Scientific) and are given in Table 1.

The samples with Beltide-1 and DMPC were also measured at the I911-SAXS beamline at MAXLab (Lund, Sweden),[33] wavelength λ = 0.91 Å in 100% H_2O based buffers at 20 °C. Data were absolute calibrated with water and reduced using the same procedure as described for the SAXS data from ESRF.

SAXS and SANS data analysis

The SAXS- and SANS data were fitted using an analytical modeling approach, where the form factor of the peptide nanodiscs was approximated by combining simple geometrical objects with known analytical form factors. The general model is described in our previous work[7,34] and the details on implementation on peptide nanodiscs are also described previously.[8] The open source program WillItFit[35] with the model PolydispersePeptideDiscs[8] was used to perform modeling, and the model is illustrated in Fig. 2. The lipid bilayer was approximated by cylindrical discs with the same diameter stacked upon each other. The top and bottom cylindrical discs represented the phospholipid head groups, the center cylinder represented the phospholipid CH_3 tail group and the cylinders in between represented the lipid CH_2 tail groups. The peptide belt was approximated using a hollow cylinder surrounding the lipid bilayer and screening the hydrophobic faces of the bilayer from the water phase. The scattering contrasts of each of these parts were calculated and included in the model. Molecular constraints were applied to minimize the number of free parameters and ensure that only physically realistic models were tested.[34]

Table 1 Peptide concentration of samples for SAXS- and SANS measurements. Measured by 280 nm absorption

	Peptide conc. [mg ml^{-1}]
Beltide-1, SAXS	0.56
Beltide-1, SANS	0.32
Beltide-2, SAXS	0.68
Beltide-2, SANS	0.50
Beltide-3, SAXS	0.40
Beltide-3, SANS	0.31

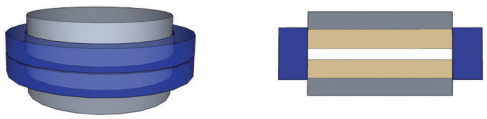

Fig. 2 3D illustration and cross section of the peptide nanodisc model. The different colors correspond to different excess scattering length densities in the disc. The peptide belts are blue, the lipid head groups are gray, the lipid CH_2 tail groups are light brown and the lipid CH_3 tail groups are white.

Light scattering

Static light scattering (SLS) and dynamic light scattering (DLS) were performed on a light scattering instrument (Brookhaven Instruments Corporation) using a laser wavelength of λ = 637 nm and was performed immediately after SEC. Time resolved measurements were conducted within 20 seconds to 5 minutes windows depending on the temperature. The particle size could be found by the DLS signal. The field autocorrelation function relates the scattered electrical field at a given time t with the field at time $t + \tau$

$$g^{(1)}(\tau) = \frac{\langle E(t)E^*(t+\tau)\rangle}{\langle E(t)E^*(t)\rangle} \quad (2)$$

and can be found from the measured intensity using the Siegert relation. The field autocorrelation function $g^{(1)}(\tau)$ falls exponentially with a mean decay rate $\bar{\Gamma}$ and for monomodal, polydisperse samples this can be estimated *via* the cumulant expansion,[36,37] where terms up to second order were used in the present study:

$$\ln\left[g^{(1)}(\tau)\right] = -\bar{\Gamma}\tau + \frac{\kappa_2\tau^2}{2!} + \cdots \quad (3)$$

The second cumulant κ_2 corresponds to the variance of the distribution around the mean decay rate. The mean diffusion constant $\bar{D}$ can be deduced by $\bar{\Gamma} = \bar{D}q^2$, with $q = (4\pi n/\lambda_0)\sin(\theta)$ where n is the refractive index, 2θ is the scattering angle and λ_0 is the laser wavelength under vacuum. The apparent radius of hydration R_h can then be found by exploiting the Stokes–Einstein relation[38] $\bar{D} = k_BT/6\pi\eta R_h$, where k_B is Boltzmann's constant, T is temperature, and η is the viscosity. Evolution of the mass of the particles could be monitored by the SLS intensity, due to the direct relationship between intensity $I(q = 0)$ and the weight averaged molecular weight M of the particles, $I(q = 0) = KcM$, where c is the concentration and K is an optical constant. This direct relation holds true when the Rayleigh–Debye–Gans (RDG) approximation is satisfied, meaning that the wavelength used should be much larger than the studied particles. In practice, the condition is fulfilled for particle sizes less than ~300 Å. Also, it is assumed that the increase in the refractive index was constant over time.[39]

Stability of bacteriorhodopsin in peptide nanodiscs

The stability of bR in the peptide nanodiscs was monitored by measuring the chromophore absorption at 550 nm. The chromophore of bR is only active when bR is natively folded. The absorption was measured using a NanoDrop 1000 spectrophotometer (Thermo Scientific).

Coarse-grained MD simulations

Coarse-grained MD simulations were performed using ESPResSo[40] and visualized using the VMD package.[41] Lipids were simulated with four beads, and each 18A unit of the dimer peptides were simulated with 42 beads (see Fig. 3) as described in detail in previous work.[8] The size of each bead was controlled by the Weeks–Chandler–Anderson potential

$$V_{\mathrm{WCA}}(r) = \begin{cases} 4\varepsilon\left(\left(\frac{a}{r}\right)^{12} - \left(\frac{a}{r}\right)^{6}\right) + \varepsilon, & \text{if } r < r_{\mathrm{c}}, \\ 0, & \text{if } r > r_{\mathrm{c}}, \end{cases} \quad (4)$$

where $r_{\mathrm{c}} = 2^{1/6}a$ is the distance at which $V_{\mathrm{WCA}} = 0$. By varying a, the self-assembly of the lipids without peptides could be controlled[42] such that they formed vesicles, as DMPC is known to do. The a between the lipid tails and the hydrophobic peptide beads was set to 0.5 to give a flat hydrophobic peptide–lipid interface. This was needed for the peptide to align as belts around the lipid bilayers. See values of a in Table 2.

No explicit solvent was simulated and the hydrophobic effect was taken into account by an additional attractive potential between the hydrophobic beads:

$$V_{\cos}(r) = \begin{cases} -\varepsilon, & \text{if } r < r_{\mathrm{c}}, \\ -\varepsilon\cos^2\left(\frac{\pi(r - r_{\mathrm{c}})}{2\omega}\right), & \text{if } r_{\mathrm{c}} < r < r_{\mathrm{c}} + \omega, \\ 0, & \text{if } r > r_{\mathrm{c}} + \omega. \end{cases} \quad (5)$$

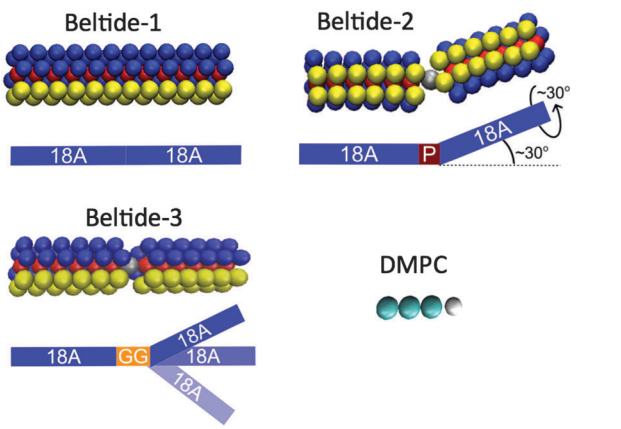

Fig. 3 Coarse-grained models of the three beltides and of DMPC. Hydrophilic peptide beads in blue and hydrophobic in yellow. The central beads are red and the linker bead is grey. The hydrophilic phospholipid head bead is white and the beads representing the hydrophobic tail group are turquoise.

Table 2 Values of a from the WCA potential between different bead types. Abbreviations: h = phospholipid head, t = phospholipid tail, p_{phil} = hydrophilic peptide, and p_{phob} = hydrophobic peptide

	h–h	h–t	h–p_{phil}	h–p_{phob}	t–t
a	0.80	0.85	0.85	0.85	1.0
	t–p_{phil}	t–p_{phob}	p_{phil}–p_{phil}	p_{phil}–p_{phob}	p_{phob}–p_{phob}
a	0.90	0.50	0.90	0.90	1.0

Following previous studies,[8,43] the energy ε was set to unity and the interactions were $\omega_{\mathrm{lipid\text{–}lipid}} = \omega_{\mathrm{peptide\text{–}lipid}} = 1.6$ and $\omega_{\mathrm{peptide\text{–}peptide}} = 0.8$.

The peptide beads and lipid tail beads had a diameter of $1\sigma_{\mathrm{MD}}$ and the head bead diameter was $0.9\sigma_{\mathrm{MD}}$, where σ_{MD} is the unit of length in the simulations. $1\sigma_{\mathrm{MD}}$ corresponds to about 5.3 Å, since the 18A peptide is 32 Å long and simulated as being 6 beads long. The interhelical linker was represented as a point through which an angle dependent harmonic bond connected the two 18A peptides into a dimer

$$V(\phi)_{\mathrm{bond}} = \frac{K}{2}(\phi - \phi_0)^2, \quad (6)$$

where the linker strength K was set to 10ε for the Gly–Gly linker and 100ε for the Pro linker, and the resting angle ϕ_0 was set to respectively 0 and 30°. The fixed twist induced by Pro was obtained by cross-linking the two 18A subunits with harmonic bonds. The bonds had different lengths, such that the 30° kink was sustained.

The total energy of the system and the number of lipids per particle were monitored as a function of time. Simulation time was converted into seconds following Illya and Deserno,[43] by comparing simulated phospholipid diffusion time with the experimental value.

Peptides and lipids were placed at random in a $(60\sigma_{\mathrm{MD}})^3$ simulation box under periodic boundary conditions. This simple initial point of the simulations was equivalent to the experimental starting point, where the lipid–peptide film was mixed with buffer without detergent. The 4-bead phospholipids matched to the length of DMPC, namely 20 Å, but the width was different, so a computational conversion factor was found by comparing the area per simulated phospholipid headgroup, 22 Å^2, with the experimentally determined area per headgroup for DMPC of 60.6 Å^2.[44] This gave a crude conversion factor of 2.7 that was used when the number of simulated phospholipids was compared to experiment. The peptide concentration of 3.3 mM correspond to 33 dimer peptides per simulation. The initial amount of simulated phospholipids per peptide in each simulation was determined from the SAXS/SANS modeling to be 53, 27 and 45 for Beltides-1, -2, and -3 respectively.

Results

Size exclusion chromatography (SEC)

SEC was performed to obtain information on the self-assembly and overall size of the particles. A scan over different phospholipid

to peptide molar stoichiometries was used to find the optimal stoichiometry to use for further studies. The optimal stoichiometry should give rise to a chromatogram with a single, narrow and symmetric peak close to 13 ml retention volume, where both MSP nanodiscs and 18A nanodiscs are known to appear. Self-assembly was investigated for a range of stoichiometries and Fig. 4 shows chromatograms for the particles prepared with DMPC and respectively Beltides-1, -2, or -3. The chromatograms were normalized by the area under the curve. High yields were observed for the optimal stoichiometries (black curves on Fig. 4) as judged by the absence of a peak at the void volume (8 ml).

Beltide-1:DMPC. Samples were prepared with 0, 3.3, 6.5, 8.5, 13.1, 17.0, and 19.6 phospholipids per peptide and the obtained chromatograms are shown in Fig. 4(A). Peaks were observed at three distinct retention volumes. The first peak appeared at the exclusion limit of the column at 8 ml and was most evident for the samples with many lipids per peptide. The peak at 17 ml, on the other hand, was only seen for the samples with few or no lipids per peptide, meaning that this peak corresponds to peptide particles without lipids. The middle peak at ~13 ml was assumed to be peptide nanodiscs. 19.6 phospholipids per peptide was the optimal stoichiometry.

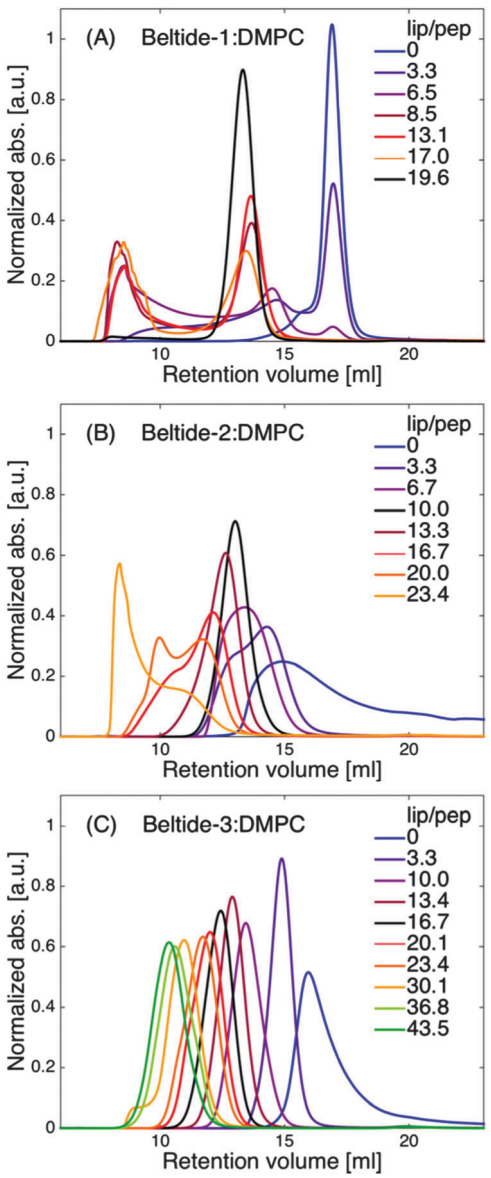

Fig. 4 Chromatograms for (A) Beltide-1:DMPC, (B) Beltide-2:DMPC and (C) Beltide-3:DMPC particles. The legends list the number of lipids per peptide, with the optimal stoichiometry in black. The chromatograms were normalized by the area under the curve.

Beltide-2:DMPC. Samples were prepared with 0, 3.3, 6.7, 10.0, 13.3, 16.7, 20.0, and 23.4 phospholipids per peptide, and the chromatograms are shown in Fig. 4(B). The overall pattern was smeared compared to the Beltide-1:DMPC chromatograms, but a peak at ~13 ml appeared for most stoichiometries. One data set with 10.0 lipids per peptide had only one narrow peak close to 13 ml, so 10.0 was the optimal stoichiometry. A ratio dependency was observed: the higher the amount of peptides, the larger the retention volume of the main peak. Several data sets, *e.g.* with 23.4, 20.0, and 16.7 lipids per peptide, are clearly sums of more than one peak, that is, the samples consisted of two or more particle sizes.

Beltide-3:DMPC. Samples with 0, 3.3, 10.0, 13.4, 16.7, 20.1, 23.4, 30.1, 36.8, and 43.5 phospholipids per peptide were measured and chromatograms are shown in Fig. 4(C). All chromatograms had one narrow, symmetric peak and the position of each peak was directly correlated with the stoichiometry, *i.e.* the more lipids per peptide, the larger the particles. The optimal stoichiometry was chosen to be 16.7, but other stoichiometries could have been chosen.

Static light scattering (SLS) stability measurements

SLS was performed to probe the structural stability of the peptide nanodiscs, *i.e.* how quickly the scattering intensity from the sample increased, corresponding to the formation of larger particles in the sample. Fig. 5 shows SLS measurements at 20 °C for particles with DMPC and, respectively, 18A, Beltides-1, -2, and -3. Experiments were performed with and without bR in the nanodiscs, such that the effect of a transmembrane protein on the structural stability could be investigated. The 18A:DMPC data from our previous paper[8] were included for comparison. Data revealed a significant variation in the stability of the peptide nanodiscs, as judged by the slope of the curves, both with and without incorporated bR. Beltide-2 nanodiscs are by far structurally most unstable. Interestingly, Beltide-1 nanodiscs are as stable as 18A nanodiscs without bR and when bR is incorporated, they are structurally more stable. The SLS signals for Beltide-3 nanodiscs were fluctuating. This could be explained by a combination of many small and a few very large particles in the sample. An increase in SLS intensity over time was seen for all peptide nanodiscs. This could be explained by growth of all particles in the sample, or by few larger aggregates emerging over time, and others still having the same structure, *i.e.* a multimodal distribution of particles. To investigate this, a sample of 18A nanodiscs was measured by SEC after 0, 4.5 and 19 hours SLS measurements at 20 °C (data not shown). The peak shifted from 13.5 ml to 13.1 ml after 4.5 hours and finally to 12.7 ml after 19 hours, so the 18A nanodiscs did indeed grow

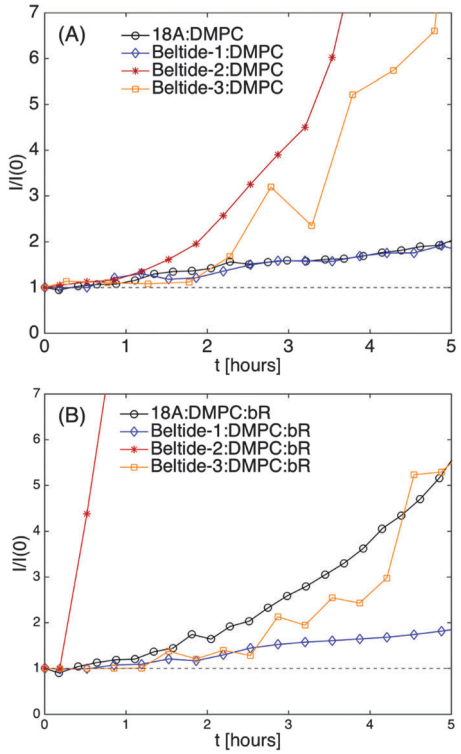

Fig. 5 SLS measured after the formation of peptide nanodiscs respectively without bR (A) and with bR (B). Data for 18A:DMPC with and without bR are plotted for easy comparison. All SLS data were measured at 20 °C, and the grey line at unity is a guide to the eye.

in size. However, this alone could not explain that the SLS intensity more than doubled within the 19 hours. That is, large particles did also appear in the sample, *i.e.* the samples developed a multimodal size distribution over time. No additional peak was observed after 4.5 or 19 hours, so these large particles either did not contain peptides, or they were large enough to end in the void volume, that is, larger than a 600 kDa protein.

SLS was also performed at 10 °C and 30 °C (data not shown) and showed that the particles aggregated faster at higher temperatures, as also observed for the 18A:DMPC system.[8] In particular it was observed that the samples developed very slowly at 10 °C for which reason this temperature was selected for further SAXS/SANS experiments.

Dynamic light scattering (DLS)

DLS measurements performed during the time scans showed that the initial hydrodynamic diameters of the peptide–lipid particles were ~100 Å, which were comparable to the typical diameter of MSP1D1 nanodiscs[45,46] and 18A nanodiscs.[8] The DLS autocorrelation data could not be fitted with a single exponential function, when the SLS intensity had increased significantly, suggesting that particles with different sizes were present in the sample, *i.e.* again consistent with a multimodal size distribution in the sample.

Circular dichroism

The CD spectra of α-helical proteins and peptides are characterized by two distinct negative minima at 208 and 222 nm,

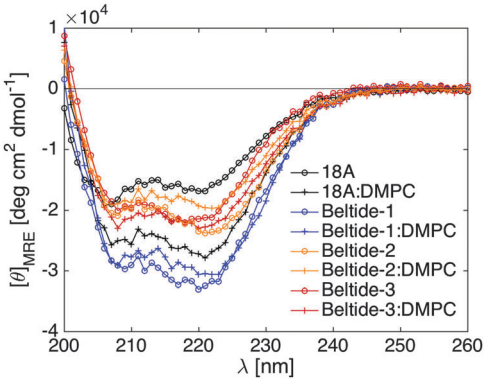

Fig. 6 Far UV CD spectra of free 18A and beltides (○) and 18A and beltides with DMPC (+). The data are shown from 200 to 260 nm as the S/N ratio was poor below this range. All beltide samples were in PBS with a concentration of ~10 μM, while 18A samples had a concentration of ~20 μM.

Table 3 Percentage helix (±standard error of the mean) in peptides and discs calculated from the mean residue ellipticity at 222 nm

	% Helix	
	Free	DMPC
18A	48.4 ± 1.1	76.7 ± 1.5
Beltide-1	89.1 ± 1.3	86.3 ± 1.2
Beltide-2	68.3 ± 1.0	58.2 ± 1.3
Beltide-3	61.1 ± 1.3	65.5 ± 1.4

and a positive maximum at 192 nm.[47] To maintain the conditions used in our other experiments, the CD measurements were carried out in PBS at 10 °C. Due to the high chloride concentration in this buffer, the signal/noise ratio was only acceptable down to around 195–200 nm in this analysis, leaving out the possibility of convincingly observing the strong positive feature at 192 nm. Based on the two distinct minima at 208 and 222 nm, however, all beltides and beltide nanodiscs were significantly helical in solution (Fig. 6).

The percentage of helix was estimated from the mean residual ellipticity at 222 nm (Table 3). Ranging from 48 to 89% helix, all peptides were highly helical both in the free form and in complex with DMPC.

Combined SAXS and SANS measurements

Small angle scattering, supplemented by modeling, provided information on the size, structure and composition of the self-assembled peptide nanodiscs. Data are plotted in Fig. 7. All data sets have a flat Guinier region at low q. SAXS data exhibit an oscillation with a local minimum at $q \sim 0.06$–0.07 Å^{-1} followed by an upturn and then a decrease to a constant level at $q > 0.3$ Å^{-1}.

***p*(*r*) functions.** In Fig. 8 the pair distance distribution functions $p(r)$ are provided for the SAXS- and SANS data. These were normalized by the area under the curve. A minimum is observed for the SAXS $p(r)$ functions at ~30 Å and can be explained by the lipid bilayer: the $p(r)$ function is weighted with the excess scattering length density, which is oscillating in the discs. It is negative for the lipid tails, but positive for the peptide belts and

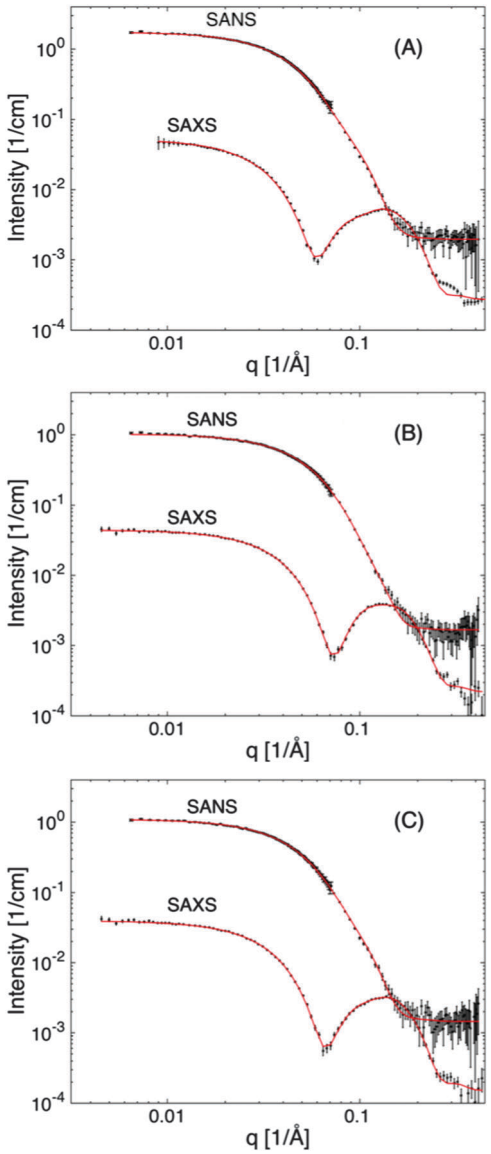

Fig. 7 Combined SAXS and SANS data for peptide nanodiscs. (A) Beltide 1 with DMPC, (B) Beltide-2 with DMPC and (C) Beltide-3 with DMPC. Data are fitted with a model of discoidal particles (Fig. 2). The fitting parameters for the model are listed in Table 4. Data were fitted with the program WillItFit.[35]

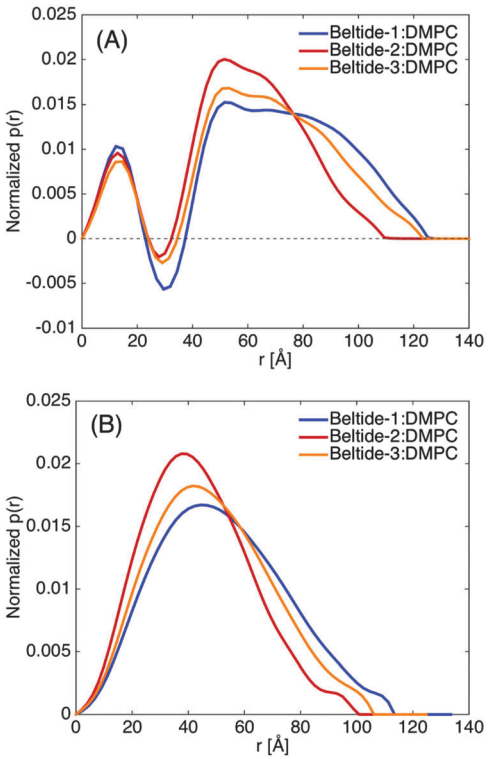

Fig. 8 $p(r)$ functions of (A) SAXS data and (B) SANS data. The data sets have been normalized with the area under the graph.

lipid heads. Because of the neutron contrast situation, this oscillatory profile is not present in SANS data. Both SAXS and SANS data indicated that the Beltide-1 nanodiscs were the largest with a maximal distance D_{max} of ~120 Å according to the SAXS data and ~110 Å according to SANS data. Beltide-2 nanodiscs had the smallest maximal distance of ~110 Å according to SAXS and ~100 Å according to SANS. The Beltide-3 nanodiscs were slightly smaller than the Beltide-1 nanodiscs.

Model fitting. A model of polydisperse circular peptide nanodiscs fitted the SAXS and SANS data excellently. The fits were accurate up to $q \sim 0.25$ Å^{-1}, showing that the model reflected the low-resolution structure. The analysis was consistent with the assumption that all three beltides with DMPC self-assembled into peptide nanodiscs. Structural information of size, shape and composition, which could be retrieved from the fitting parameters, is listed in Table 4. The relative polydispersity, *i.e.* the variation of the number of lipids per peptide nanodisc, was comparable for the three peptide nanodiscs, namely $\sigma_{rel} \approx 0.2$, where σ_{rel} is the relative standard deviation of a normal distribution describing the number of lipids per nanodisc in the sample.[35] The model included nanodiscs with different sizes, but all having the same width of the beltides. However, the values of mean no. of lipids per disc, mean diameter of the disc, mean no. of peptides per disc and lipids per peptides in the disc listed in Table 4 are all peak-values, *i.e.* values for the most common nanodisc in the distribution. However, because of the narrow size-distributions, the mean values for the entire distribution only deviates slightly from the peak-values. For Beltide-1:DMPC the mean and peak values are respectively 288.2 and 288.2 lipids per disc, 26.4 and 26.6 lipids per peptide, and 10.9 and 10.8 peptides per disc.

Number of lipids

The number of lipids per peptide in the sample before SEC was known, and it differed from the stoichiometry found by SAS modelling. For example, the initial sample stoichiometry for Beltide-1:DMPC was 19.6 lipids per peptide and the stoichiometry found by SAS modelling was 26.4, *i.e.* there were more lipids per peptide in the peptide nanodiscs than in the initial sample. This was also seen for Beltide-2:DMPC, Beltide-3:DMPC and 18A:DMPC, showing that some peptides are lost during the formation of nanodiscs.

Table 4 Parameters from fitting the peptide nanodisc model simultaneously to SAXS and SANS data. The 95% confidence interval (C.I.) is listed

	Beltide-1:DMPC		Beltide-2:DMPC		Beltide-3:DMPC	
Refined Parameters	Value	C.I. 95%	Value	C.I. 95%	Value	C.I. 95%
Area per headgroup [Å^2]	53.6	51.7–56.1	52.7	49.2–56.4	50.8	47.4–54.5
Mean no. of lipids per disc	288	258–308	164	152–177	243	225–263
Width of belt [Å]	7.3	5.8–8.3	9.6	8.2–11.4	9.8	8.8–10.8
$\sigma_{\text{No.lipids,relative}}$	0.22	0.00–0.38	0.24	0.00–0.48	0.23	0.00–0.39
Volume of a single lipid [Å^3]	1085	1074–1091	1074	1064–1084	1068	1057–1078
Volume of a single peptide [Å^3]	5340	5012–5816	5714	5144–6133	5733	5337–6119
	Beltide-1:DMPC		Beltide-2:DMPC		Beltide-3:DMPC	
Derived parameters	Value	C.I. 95%	Value	C.I. 95%	Value	C.I. 95%
Mean diameter of disc [Å]	114	—	93	—	108	—
Mean no. of peptides per disc	10.9	—	10.5	—	12.6	—
Lipids per peptide in disc	26.4	—	15.6	—	19.4	—
	Beltide-1:DMPC		Beltide-2:DMPC		Beltide-3:DMPC	
Quality of fit	Value	C.I. 95%	Value	C.I. 95%	Value	C.I. 95%
Reduced χ^2	2.14	—	1.06	—	0.92	—

Coarse-grained molecular dynamics simulations

Three MD simulations were set up, corresponding to the three systems with DMPC and Beltides-1, -2, and -3 respectively. Fig. 9 shows snapshots from one simulation with Beltide-3 and DMPC. Visual inspection reveals rapid formation of intermediate lipid–peptide particles within the first few μs and in about 2 ms most of these particles merged to form peptide nanodiscs.

The systems converged rapidly with respect to total energy, as shown in Fig. 10. Note the linear behavior of the total energy on a log–log scale, indicating that the total energy in the simulations converged approximately as $E_{\text{total}} = t^b$, where t is the time and b is the slope on the log–log plot.

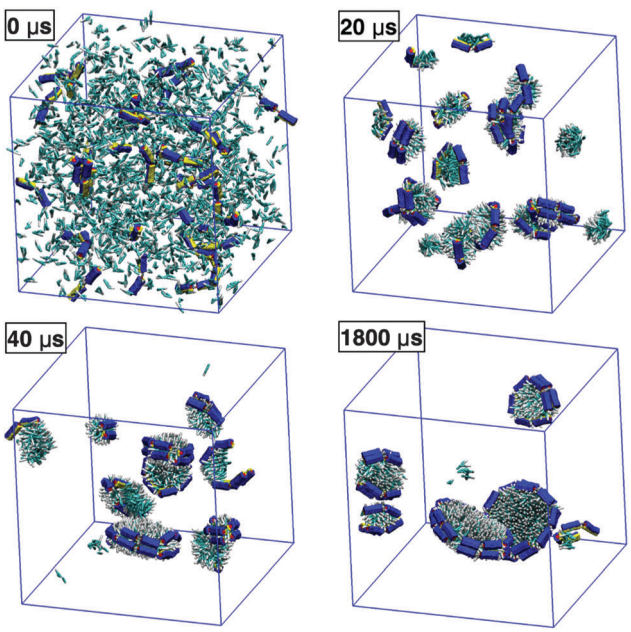

Fig. 9 Simulation snapshots for Beltide-2 with DMPC at time 0, 20, 40 and 1800 μs. The peptides and phospholipids self-assembled by a quick formation of small, intermediate lipid–peptide particles that merged to form peptide nanodiscs within about 2 ms.

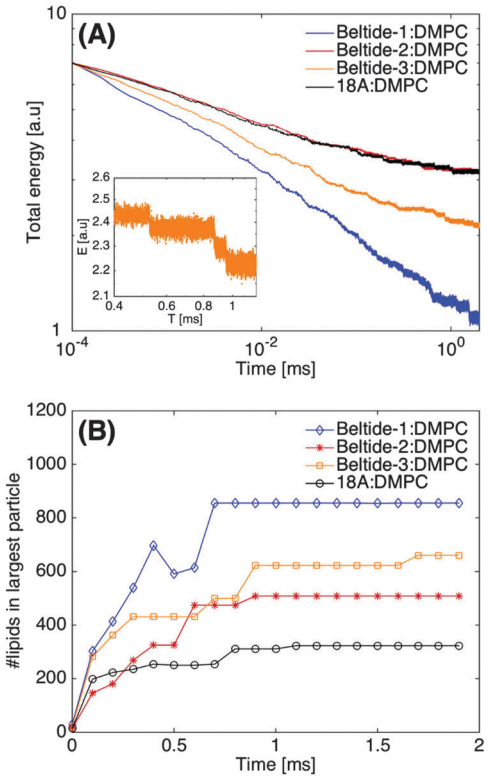

Fig. 10 The total energy of the systems (A), averaged over two simulations. The inset shows how the energy falls stepwise, reflecting that particles merge to form peptide nanodiscs. This stepwise behavior is lost when the curves are averaged. The number of lipids in the largest particles (B) converges after 1.1 ms.

The largest particles in the simulations (Fig. 11) had diameters that corresponded well with the small-angle scattering data, but the polydispersity was higher in the simulations. On a longer timescale, the simulations might converge to a less

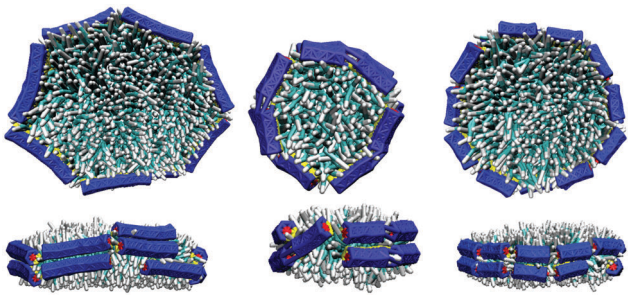

Fig. 11 Top view and side view of the peptide nanodiscs with, from left to right, Beltides-1, -2 and -3. Approximate diameters, as estimated from the simulations, are ~150, ~104 and ~120 Å respectively. The side view shows the different belt alignments.

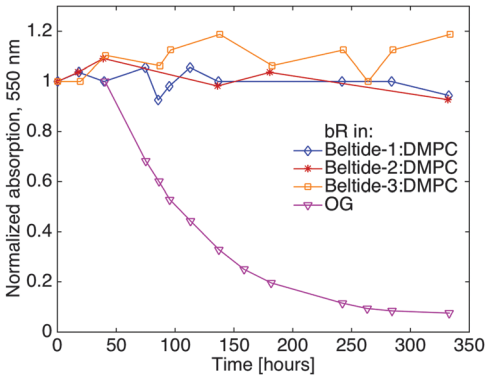

Fig. 12 bR activity monitored by 550 nm absorption at 20 °C. When bR unfolds, its chromophore becomes inactive and the absorption decreases, as seen for bR in OG micelles.

polydisperse ensemble. However, this was not practically possible to investigate, due to long simulation time. The simulations represent the first few ms, whereas the self-assembly in the experiment took place over night at 37 °C. Therefore, it seems reasonable to compare experiments only with the largest particles in the simulation. The number of lipids corresponded very well with the experimental data. As seen in Fig. 10, the mean number of lipids for the largest particles were respectively 317, 163, and 245 for Beltides-1, -2 and -3 nanodiscs (corresponding to 855, 439, and 661 simulated lipids). This should be compared to the number of lipids from SAS modelling, as listed in Table 4, namely 288, 164 and 243 respectively. The diameters of the discs were found in simulations to be ~150, ~104, and ~120 Å for peptide nanodiscs with Beltides-1, -2, and -3 respectively and SAS modelling gave 114, 93, and 108 Å, *i.e.* 25% smaller for Beltide-1 nanodiscs and 10% for Beltides-2 and -3. So the largest particles from the simulations were qualitatively consistent with the SAS models but slightly larger. Despite being larger, the simulated particles had almost the exact same number of phospholipids per disc as the SAS models. This means that the conversion factor of 2.7 between simulated and real DMPC molecules is overestimated. The area per headgroup for DMPC in unilamellar vesicles (60.6 $Å^2$) was used to calculate the conversion factor, and the SAS models had a smaller area per headgroup (54, 53 and 51 $Å^2$ respectively). Using that would give a smaller conversion factor of 2.4 and a consistent picture of the largest simulated particles being qualitatively equal to, but slightly larger than the SAS models. Monitoring the energy for the whole simulated system showed firstly the stepwise decrease in energy, as shown in the inset in Fig. 10(A), corresponding to merging of particles, and secondly, it showed the final total energy, which correlates well with the stability of the dimer peptide nanodiscs, as judged by SLS, such that the particles with lowest final energy were most stable and *vice versa*. However, this correlation between final energy and stability was not seen for the 18A nanodiscs, which had a total energy in the simulations that was remarkably similar to Beltide-2 nanodiscs, even though the 18A nanodiscs were significantly more stable.

Stabilization of bacteriorhodopsin

The stability of bR reconstituted in the three peptide nanodiscs and in OG micelles was monitored by measuring the chromophore absorption of bR at 550 nm. When bR unfolds, the absorption decreases. Fig. 12 shows that bR was stable for more than 300 hours in the peptide nanodiscs at 20 °C whereas the absorption dropped rapidly for bR in OG detergent. At 5 °C bR was stable both in OG and in the peptide nanodiscs over the measured time interval. As seen from the light scattering experiments plotted in Fig. 5, the bR-loaded beltide nanodiscs were not structurally stable at 20 °C. Therefore, samples were taken from the top layer of the tube to avoid sedimented aggregates and the spectrum was checked for the scattering signal, but no such signal was observed.

Discussion

Self-assembly

SEC showed that the self-assembly was highly affected by the linkers in the beltides. Beltide-3, with the most flexible linker, Gly–Gly, gave rise to a single symmetric SEC peak for all tested molar stoichiometries, showing that the peptide belt adapted its size to different number of lipids per peptide. Beltide-1, on the other hand, was very non-adaptable, so several SEC peaks were observed for each stoichiometry. Not surprisingly, Beltide-2 with the semi-flexible Pro linker exhibited a semi-adaptable behavior. Monomeric 18A was very adaptable (data not shown), similar to Beltide-3, reflecting that the absence of the linker gave high flexibility. Coarse-grained MD simulations gave detailed insight into the self-assembly, with hydrophobic attraction between the molecules as the main driving force. The beltides and the phospholipids aggregated into small peptide–lipid particles within few μs and the total energy of the system also decreased very rapidly. These particles then merged by collisions and the first full-sized peptide nanodiscs were formed within about 1 ms. The self-assembly slowed down with less frequent collisions and after about 2 ms, there were still particles in the solution that had not reached the full size. The initial- and final states of the simulation were consistent with experiment, which is a required condition to trust the simulations.

Secondary structure

In previous work, 18A was found to be 55% helical in the free form, and 72% in complex with DMPC estimated from the

mean residueal ellipticity at 222 nm.[26] In another study, 18A was 38% helical in the free form and up to 92% helical in complex with DMPC depending on the peptide:lipid ratio. In our study, 18A was estimated to be 48% helical in the free form and 77% in complex with DMPC, which was in good accordance with the previous data. Interestingly, the high helix content of Beltide-1 was close to invariant between the free peptide (89%) and the complex with DMPC (86%). This indicated that the secondary structure of free Beltide-1 was far more stable than that of free 18A. As expected, the proline and glycine containing Beltide-2 and Beltide-3 were less helical than Beltide-1 due to the helix puncturing residues. The slightly lower helicity of Beltide-3 compared to Beltide-2 is in accordance with the presence of two glycines in the first and only one proline in the latter. 37 pA, a model peptide with the same sequence as Beltide-2 but without chemical modification of the termini, was previously found to be 26–28% helical alone and 34% helical in complex with DMPC.[27,28] Here, Beltide-2 was estimated to be 68% helical alone and 58% in complex with DMPC. N-terminal acetylation and C-terminal amidation of 18A significantly stabilized the peptide, which resulted in an increase of helicity from 6 to 38%.[27] It is noteworthy that the previous experiments were carried out under different conditions, particularly at higher temperatures, but given a more than two-fold increase in helicity from 37 pA to Beltide-2, our results indicated that the chemically modified termini provided significant stability. For Beltide-2, we found a significant loss of helicity when complexed to DMPC. In the work by Sethi *et al.*,[28] the presented CD spectra indicate a slight loss of helicity for 37 pA when complexed with DMPC, although they report an increase in helicity. A decrease in helicity is in accordance with our results. This result could indicate that Beltide-2 must undergo a conformational change to adopt an adequate hydrophobic match with the lipids. Beltide-3 was estimated to be 61% helical alone and 65.5% in complex with DMPC. This indicates that the probably highly flexible glycine linker is slightly stabilized upon DMPC binding. Thus, the CD data indicated that Beltide-1 and Beltide-3 underwent no or subtle conformational rearrangements when binding DMPC, whereas 18A gained a substantial amount of helix, and Beltide-2 lost a small amount of helix. Our results confirmed previous findings that chemical modification of the termini contributes favorably to the stability of α-helical peptides.

Nanodisc structure

SAXS and SANS data were consistent with a model of slightly polydisperse peptide nanodiscs composed of a flat lipid bilayer, with a belt of peptides screening the hydrophobic side of the bilayer (Fig. 2), *i.e.* the same model that described the 18A nanodiscs.[8] Comparison of the derived model parameters showed that different linkers resulted in difference in size, with Beltide-1 nanodiscs being the largest and Beltide-2 nanodiscs being the smallest. Beltide-3 did not confine the size of the formed peptide nanodiscs due to its adaptability and the size could be controlled by changing the lipid–peptide stoichiometry of the sample. The largest particles from the coarse-grained MD simulations were qualitatively consistent with the SAS models but slightly larger. The SAS modelling suggested that the peptide nanodiscs all had a relative polydispersity of 0.2 (see Table 4). The dimeric beltide nanodiscs were expected to be more polydisperse than MSP1D1 nanodiscs,[6,34,45] but interestingly the analysis suggested that they were less polydisperse than 18A peptide nanodiscs with a relative polydispersity of 0.4.[8] The optimal composition of the discs differed, which can be seen from the extracted model parameters in Table 4. The nanodiscs with Beltide-1 and DMPC had fewer peptides per lipid than discs with Beltides-2 and -3. This is a natural consequence of the difference in size and the fact that the number of phospholipids scales with the area, and the number of peptides scales with the circumference. It was expected that larger nanodiscs would contain more beltides. The size order including the 18A nanodiscs was: 18A nanodiscs → Beltide-2 nanodiscs → Beltide-3 nanodiscs → Beltide-1 nanodiscs. The number of beltides per nanodisc was (listed in the same order): 15 → 21 → 25 → 22. So Beltide-1 nanodiscs had fewer peptides per disc than expected. Furthermore, the width of Beltide-1 was only 7.3 Å, as compared to 9.6 and 9.8 Å for Beltides-2 and -3 respectively. This can be explained by Beltide-1 forming both single belts and double belts at the rim of the nanodisc, and not only double belts as assumed in the model. The discrepancy between the model and the sample was then compensated for by decreasing the number of peptides per disc and the thickness of the belt. Coarse-grained MD simulations also indicated the presence of single belt formation in addition to the double belt, as seen in Fig. 11, however not to a higher degree for Beltide-1 than for Beltides-2 or -3.

Structural stability and ability to stabilize membrane proteins

SLS showed a structural change of the sample over time, and the structural stability could be assessed by the slope of the SLS curves. A correlation between size and stability of the formed nanodiscs was observed: Beltide-2 nanodiscs were smallest and least stable, whereas Beltide-1 nanodiscs were the largest and most stable.

The stability of the beltide nanodiscs was reflected in the energy of the system, as monitored in the MD simulations, see Fig. 10. The simulations converged to different total energies and these energies correlated well with the stability of the systems, such that Beltide-1 nanodiscs were most stable and reached the lowest energy, and Beltide-2 nanodiscs were most unstable and converged to the highest energy. However, this was not true for the 18A nanodiscs, which had the same total energy as the Beltide-2 nanodiscs, but where more stable, as judged by the slope of the SLS curves.

In our previous work,[8] we showed that 18A nanodiscs are structurally less stable than apoA1-based MSP1D1 nanodiscs, and a motivation for investigating the two-helical beltides was to find a system that was structurally more stable than the 18A nanodiscs. By having two linked helical segments, the dimer peptides bridge part of the gap between the 18A peptides with one helical segment and MSP with ten helical segments. Beltide-1 nanodiscs were shown to be structurally more stable than the 18A nanodiscs, when bR was embedded in the nanodiscs,

indicating that higher structural stability can be obtained by increasing the subsequent helical units per beltide.

All three peptide nanodiscs stabilized the 7 transmembrane protein bR equally well and significantly better than OG at 20 °C, meaning that the nanodiscs have great potential as systems for handling membrane proteins.

The role of interhelical linkers in apoA1 and its effect on nascent HDL

Due to the similarity between the beltides and apoA1, the study gave insight into the role of the interhelical linkers in apoA1, the main protein constituent of nascent discoidal high density lipoproteins (HDL). The Pro linker, which is present in seven out of ten helices in apoA1, had a 30° kink that confined the formed Beltide-2 nanodiscs to a specific size, corresponding to a SEC peak around 13 ml on the Superdex 200 column. The size of HDL is shown to be important for its function,[48] so one main function of Pro is possible to confine the HDL particles in size. The Gly–Gly linker induced more adaptability and we hypothesize that it provides structural flexibility in apoA1, meaning that it can change dynamically between different states, such as those suggested by Mei and Atkinson.[49] Hence, Pro and Gly–Gly have opposite effects as linkers, *i.e.* Pro linkers confine the formed HDL particle to a specific size, whereas Gly–Gly linkers give structural variability.

Conclusion

We studied three dimer peptides: Beltide-1, which contained two copies of 18A with no linker, Beltide-2 with the two copies of 18A linked by Pro, and Beltide-3 with the two copies of 18A linked by Gly–Gly. CD spectroscopy showed that all peptides were helical in the free form and when bound to DMPC. It was found that all three self-assembled with DMPC to slightly polydisperse, circular peptide nanodiscs, as revealed by combined SAXS and SANS and coarse-grained MD simulations. The nanodiscs were more polydisperse than MSP nanodiscs but less than 18A nanodiscs. Interestingly, all peptides had a diameter between 100 and 150 Å, as seen for similar systems, such as 18A nanodiscs, MSP nanodiscs, polymer SMALP discs[4] and other apoA1 mimicking peptide nanodisc systems with different peptide architectures.[22] Even though the overall structure was the same for all the beltides, the linkers affected the size of the formed peptide nanodiscs with Beltide-1 nanodiscs being the largest and Beltide-2 nanodiscs being the smallest. Coarse-grained MD simulations were consistent with the SAS data and gave insight into the timescale of the self-assembly, showing how small, intermediate particles merged to form peptide nanodiscs within few ms. The presence of an interhelical linker affected the adaptability of the peptide dimers, so the peptide belt could adapt to different lipid–peptide stoichiometries. Beltide-3 was very adaptable and several peptide–lipid stoichiometries gave single, symmetric SEC peaks, while Beltides-1 and -2 were not very adaptable.

The linkers also affected the structural stability of the formed peptide nanodiscs, meaning that the nanodiscs with the rigid Beltide-1 were more stable than the two other peptide nanodiscs. It is noteworthy that when bR was incorporated, Beltide-1 nanodiscs were more stable than 18A nanodiscs, showing that it is possible to increase structural stability by increasing the length of the peptide, and thereby bridging the gap between the dynamic 18A nanodiscs with one helical unit and the stable MSP nanodiscs with 10 helical units. This structural stability could have an effect on the ability to stabilize membrane proteins.

It was shown that the peptide nanodiscs could stabilize bacteriorhodopsin much better than OG micelles at 20 °C, so the peptide nanodiscs have great potential as a system for easy handling of membrane proteins.

Both the Pro linker and the double Gly linker are present in the apoA1 sequence. The Pro linkers confine the HDL particles to a specific size by inducing a 30° kink between the helices, and the Gly–Gly linker provides the flexibility that is needed in order to change between different states. This way, the two linkers balance each other.

We conclude that it is possible to tune stability, adaptability, size and polydispersity of peptide nanodiscs by using beltides of different lengths and with different interhelical linkers.

Acknowledgements

The authors would like to thank ILL (D11), ESRF (BM29) and MAX-lab(I911-SAXS) for beamtime and support. We also thank Peter Thulstrup (Department of Chemistry, University of Copenhagen) for measuring time at their CD spectrometer. We thank Martin C. Pedersen and Jens B. Simonsen for helpful discussion, and finally, we thank the CoNeXT 2016 program, DanScatt and the Danish Council for Independent Research for the co-funding of the project.

References

1 J. P. Overington, B. Al-Lazikani and A. L. Hopkins, *Nat. Rev. Drug Discovery*, 2006, **5**, 993–996.
2 C. Tribet, R. Audebert and J. L. Popot, *Proc. Natl. Acad. Sci. U. S. A.*, 1996, **93**, 15047–15050.
3 A. Diller, C. Loudet, F. Aussenac, G. Raffard, S. Fournier, M. Laguerre, A. Grélard, S. J. Opella, F. M. Marassi and E. J. Dufourc, *Biochimie*, 2009, **91**, 744–751.
4 T. J. Knowles, R. Finka, C. Smith, Y.-P. Lin, T. Dafforn and M. Overduin, *J. Am. Chem. Soc.*, 2009, **131**, 7484–7485.
5 T. H. Bayburt and S. G. Sligar, *FEBS Lett.*, 2009, **584**, 1721–1727.
6 T. H. Bayburt, Y. V. Grinkova and S. G. Sligar, *Nano Lett.*, 2002, **2**, 853–856.
7 N. Skar-Gislinge, J. B. Simonsen, K. Mortensen, R. Feidenhans'l, S. G. Sligar, B. Lindberg Møller, T. Bjørnholm and L. Arleth, *J. Am. Chem. Soc.*, 2010, **132**, 13713–13722.
8 S. R. Midtgaard, M. C. Pedersen, J. J. K. Kirkensgaard, K. K. Sørensen, K. Mortensen, K. J. Jensen and L. Arleth, *Soft Matter*, 2014, **10**, 738–752.

9 P. Kanellis, Y. Romans, B. J. Johnson, H. Kercret, R. Chiovetti, T. M. Allen and J. P. Segrest, *J. Biol. Chem.*, 1980, **255**, 11464–11472.
10 G. M. Anantharamaiah, J. L. Jones, C. G. Brouillettes, C. F. Schmidt, B. H. Chung, T. A. Hughes, A. S. Bhown and J. P. Segrest, *J. Biol. Chem.*, 1985, **260**, 10248–10255.
11 G. Datta, M. Chaddha, S. Hama, M. Navab, A. M. Fogelman, D. W. Garber, V. K. Mishra, R. M. Epand, R. F. Epand, S. Lund-Katz, M. C. Phillips, J. P. Segrest and G. M. Anantharamaiah, *J. Lipid Res.*, 2001, **42**, 1096–1104.
12 V. K. Mishra, M. N. Palgunachari, R. Krishna, J. Glushka, J. P. Segrest and G. M. Anantharamaiah, *J. Biol. Chem.*, 2008, **283**, 34393–34402.
13 G. D. Wool, C. A. Reardon and G. S. Getz, *J. Lipid Res.*, 2008, **49**, 1268–1283.
14 C. B. Sherman, S. J. Peterson and W. H. Frishman, *Cardiol. Rev.*, 2010, **18**, 141–147.
15 V. K. Mishra, G. M. Anantharamaiah, J. P. Segrest, M. N. Palgunachari, M. Chaddha, S. W. S. Sham and N. R. Krishna, *J. Biol. Chem.*, 2006, **281**, 6511–6519.
16 C. N. Pace and J. M. Scholtz, *Biophys. J.*, 1998, **75**, 422–427.
17 J. Rankenberg, V. Vostrikov, C. DuVall, D. Greathouse, R. Koeppe II, C. Grant and J. Opella, *Biochemistry*, 2012, **51**, 3554–3564.
18 S. C. Lovell, I. W. Davis, W. B. Arendall III, P. I. W. de Bakker, J. M. Word, M. G. Prisant, J. S. Richardson and D. C. Richardson, *Proteins*, 2003, **50**, 437–450.
19 V. K. Mishra, M. N. Palgunachari, S. Lund-Katz, M. C. Phillips, J. P. Segrest and G. M. Anantharamaiah, *J. Biol. Chem.*, 1995, **270**, 1602–1611.
20 B. H. Chung, G. M. Anatharamaiah, C. G. Brouillettes, T. Nishidag and J. P. Segrest, *J. Biol. Chem.*, 1985, **260**, 10256–10262.
21 Y. V. Venkatachalapathi, M. C. Phillips, R. M. Epand, R. F. Epand, E. M. Tytler, J. P. Segrest and G. M. Anantharamaiah, *Proteins*, 1993, **15**, 349–359.
22 Y. Zhao, T. Imura, L. J. Leman, L. K. Curtiss, B. E. Maryanoff and M. R. Ghadiri, *J. Am. Chem. Soc.*, 2013, **135**, 13414–13424.
23 H. Kariyazono, R. Nadai, R. Miyajima, Y. Takechi-Haraya, T. Baba, A. Shigenaga, K. Okuhira, A. Otaka and H. Saito, *Pept. Sci.*, 2016, **22**, 116–122.
24 D. Oesterhelt and W. Stoeckenius, *Methods Enzymol.*, 1974, **31**, 667–678.
25 N. Dencher and M. Heyn, *Methods Enzymol.*, 1982, **88**, 5–10.
26 V. K. Mishra, M. N. Palgunachari, J. P. Segrest and G. M. Anantharamaiah, *J. Biol. Chem.*, 1994, **269**, 7185–7191.
27 J. A. Gazzara, M. C. Phillips, S. Lund-Katz, M. N. Palgunachari, J. P. Segrest, G. M. Anantharamaiah and J. W. Snow, *J. Lipid Res.*, 1997, **38**, 2134–2146.
28 A. A. Sethi, J. A. Stonik, F. Thomas, S. J. Demosky, M. Amar, E. Neufeld, H. B. Brewer, W. S. Davidson, W. D'Souza, D. Sviridov and A. T. Remaley, *J. Biol. Chem.*, 2008, **283**, 32273–32282.
29 P. Pernot, A. Round, R. Barrett, A. De Maria Antolinos, A. Gobbo, E. Gordon, J. Huet, J. Kieffer, M. Lentini, M. Mattenet, C. Morawe, C. Mueller-Dieckmann, S. Ohlsson, W. Schmid, J. Surr, P. Theveneau, L. Zerrad and S. McSweeney, *J. Synchrotron Radiat.*, 2013, **20**, 660–664.
30 K. Lieutenant, P. Lindner and R. Gahler, *J. Appl. Crystallogr.*, 2007, **40**, 1056–1063.
31 P. Pernot, P. Theveneau, T. Giraud, R. N. Fernandes, D. Nurizzo, D. Spruce, J. Surr, S. McSweeney, A. Round, F. Felisaz, L. Foedinger, A. Gobbo, J. Huet, C. Villard and F. Cipriani, *J. Phys.: Conf. Ser.*, 2010, **247**, 012009.
32 S. Hansen, *J. Appl. Crystallogr.*, 2012, **45**, 566–567.
33 A. Labrador, Y. Cerenius, C. Svensson, K. Theodor and T. Plivelic, *J. Phys.: Conf. Ser.*, 2013, **425**, 072019.
34 N. Skar-Gislinge and L. Arleth, *Phys. Chem. Chem. Phys.*, 2011, **13**, 3161–3170.
35 M. C. Pedersen, L. Arleth and K. Mortensen, *J. Appl. Crystallogr.*, 2013, **46**, 1894–1898.
36 D. E. Koppel, *J. Chem. Phys.*, 1972, **57**, 4814.
37 B. J. Frisken, *Appl. Opt.*, 2001, **40**, 4087–4091.
38 P. Pusey, *Neutrons, X-rays and Light Scattering Methods Applied to Soft Condensed Matter*, North-Holland Delta Series, 1st edn, 2002, p. 214.
39 P. Pusey, *Neutrons, X-rays and Light: Scattering Methods Applied to Soft Condensed Matter*, North-Holland Delta Series, 1st edn, 2002, pp. 16–17.
40 H. Limbach, A. Arnold, B. Mann and C. Holm, *Comput. Phys. Commun.*, 2006, **174**, 704–727.
41 W. Humphrey, A. Dalke and K. Schulten, *J. Mol. Graphics*, 1996, **14**, 33–38.
42 I. R. Cooke and M. Deserno, *Biophys. J.*, 2006, **91**, 487–495.
43 G. Illya and M. Deserno, *Biophys. J.*, 2008, **95**, 4163–4173.
44 N. Kucerka, Y. Liu, N. Chu, H. I. Petrache, S. Tristram-Nagle and J. F. Nagle, *Biophys. J.*, 2005, **88**, 2626–2637.
45 I. G. Denisov, Y. V. Grinkova, A. A. Lazarides and S. G. Sligar, *J. Am. Chem. Soc.*, 2004, **126**, 3477–3487.
46 I. G. Denisov, M. a. McLean, A. W. Shaw, Y. V. Grinkova and S. G. Sligar, *J. Phys. Chem. B*, 2005, **109**, 15580–15588.
47 S. M. Kelly, T. J. Jess and N. C. Price, *Biochim. Biophys. Acta*, 2005, **1751**, 119–139.
48 A. Pascot, I. Lemieux, D. Prud'homme, A. Tremblay, A. Nadeau, C. Couillard, J. Bergeron, B. Lamarche and J. P. Després, *J. Lipid Res.*, 2001, **42**, 2007–2014.
49 X. Mei and D. Atkinson, *J. Biol. Chem.*, 2011, **286**, 38570–38582.